Open Access Online Journal on Astronomy and Astrophysics

Acta Astrophysica Taurica

www.astrophysicatauricum.org

Acta Astrophys. Tau. 4(3), 11–15 (2023) doi:10.34898/aat.vol4.iss3.pp11-15

FU Orionis-type luminosity burst induced by a close encounter with a sub-solar mass object

A. Skliarevskii

Research Institute of Physics, Southern Federal University, Rostov-on-Don 344090, Russia
e-mail: sklyarevskiy@sfedu.ru

Received 1 November 2022

ABSTRACT

FU Ori-type objects (FUors) are characterized by short (decades- or centuries-long) episodic accretion bursts, during which their luminosity increases by orders of magnitude. A possible cause of such events is gravitational interaction between encountering stars and their disks. Numerical simulations show that this scenario requires a close approach of several to several tens of au to reproduce relatively short, year-scale, characteristic times of luminosity rise via the release of gravitational energy. However, objects in FUor binaries (including FU Orionis itself) are usually hundreds of au away from each other.

Then, relative velocities of sources, which can be estimated from the known burst duration timescales, should have been by at least an order of magnitude higher than the observed velocity dispersion in young stellar clusters. Thus, the burst onset either has a delay after the closest approach or bursts should be initiated due to a mechanism that is different from a direct gravitational mass and angular momentum exchange during a close encounter. We used numerical hydrodynamic simulations to model the possible mechanisms of luminosity burst development during the encounter between a star plus a disk system and a diskless intruder star perturbing the target system. It was found that the encounter can lead to accretion bursts even in models having a large periastron distance ($\simeq$ 500 au) between the intruder and the target. The delay between the closest approach and the burst onset is more than 4000 years. The target disk perturbation caused by the intruder flyby resulted in the development of magneto-rotational instability in the innermost parts of the disk. This mechanism can resolve the problem of coplanar FUor binaries having large distance between the companions.

Key words: accretion disks, protoplanetary disks, bursts of accretion, FUors, numerical simulations

1 Introduction

Protostars in young stellar systems are known to be subjects to a sudden increase in brightness. Such an increase can reach several orders of magnitude, while a typical timescale for a burst is tens to hundreds of years. The first discovered object – FU Orionis – formed the basis of the class of events known as FU Orionis-type eruptions. Although the number of objects classified as FUors up to date is just several tens (see, e.g., Audard et al., 2014), these events are not to be considered as rare. Young stars during their evolution probably experience ten or even several tens of outburst events (Kenyon, 1999). Outbursts of FU Orionis type are more likely to occur in the early phases of disk evolution when the disk is optically thick and active (Vorobyov and Basu, 2015; Mercer and Stamatellos, 2017).

Bursts affect disk evolution and structure, and especially its temperature characteristics. Moreover, a disk chemical composition is sensitive to both increased temperature and irradiation (Visser et al., 2015; Rab et al., 2017; Molyarova et al., 2018; Wiebe et al., 2019). Besides chemical reactions, a temperature change can lead to a shift of snowlines, the grain properties, and thus disk observational manifestations are also affected (Banzatti et al., 2015; Schoonenberg and Ormel, 2017). For instance, it was shown that a change in spectral index distribution can survive (depending on a disk characteristics) even thousands of years (Vorobyov et al., 2022). A rapid significant luminosity increase can trigger a number of instabilities. Even the dynamics of a disk possibly changes, and we can distinguish between the different mechanisms led to a burst (Vorobyov et al., 2021).

Despite the significance of outbursts and the amount of work already done on the topic, there is no consensus on the origin of such events. Multiple hypotheses have been proposed to describe the mechanisms leading to the development of a burst. Bursts are likely to occur due to an episodic increase in the rate of mass accretion from the disk to the star (Audard et al., 2014; Connelley and Reipurth, 2018). Magneto-rotational instability (MRI) is widely considered as a mechanism that provides a sufficient increase in the mass accretion rate (see, e.g., Armitage et al., 2001) when the temperature in the inner disk is high enough for the ther-

mal ionization of alkaline species. The accretion rate and the corresponding energy release as accretion luminosity during the infall of a massive clump onto the star can reach the values that are characteristic of FUors (Vorobyov, 2009). Another possible mechanism is the mass exchange between a protostar and a planet circulating around on a low orbit, as suggested in Nayakshin and Lodato (2012). Simulations show that close encounters of two stellar sources can give FUor-like accretion characteristics (Pfalzner, 2008).

FU Orionis is a binary system consisting of the north and south sources. One of the stars has been in the burst phase since 1937, when its luminosity had increased on a year scale by two orders of magnitude, while the other star still remains to be in the "quiescent" phase. Thus, it is attractive to suggest that the origin of the FU Orionis burst is a release of the gravitational energy during the passage of the closest approach point. However, the in-plane or low-inclined collision (which seems to be the case in FU Orionis) requires a very close approach (from several to couple tens of au) to reproduce the burst magnitude (Pérez et al., 2020). Considering the FU Orionis spatial geometry, we must be very careful with this assumption. The problem is that the estimated distance between the FU Orionis stars is about 250 au (Pérez et al., 2020). Then, following the logic presented in Liu et al. (2017), we can estimate the average relative velocity of the sources since we know the instance of the burst initialization (i.e., the supposed moment of the close approach). The resulting relative velocity has to be no less than 10 km s^{-1}, which is almost an order of magnitude higher than the velocity dispersion in young stellar clusters. This paradox can be solved assuming a larger periastron distance between the intruder and the target or a delay between the closest flyby and the burst onset. However, the factors determining the delay duration are yet to be discovered. Moreover, the mechanism responsible for the burst ignition probably differs from the simple gravitational interaction of objects. We aim to study the possibility of burst events in binary systems with large periastrons and delayed burst initialization.

In this work we present the results of the numerical hydrodynamic simulations of the close encounter between the two sub-solar mass sources having large periastron. The encounter is followed by the delayed FUor-like luminosity burst. The simulations show the possible scenario of the indirect burst initialization, which can account for FUors in binaries with large distances between stars.

2 Results

We use hydrodynamic modeling to study protoplanetary disks and in particular FUor phenomena. In this section we provide the basic information on the model, initial conditions and distributions of the simulations, and present the modeling results.

2.1 Brief model description

The hydrodynamic simulations were carried out using the numerical hydrodynamics code "Formation and Evolution of Stars and Disks" (FEOSAD). This code allows for simulation of a protoplanetary disk (together with a star) in the 2D-thin disk approximation on the evolutionary scales (from hundreds of kyr to several Myr). The model is presented and described in detail in Vorobyov et al. (2018). Here, we mention its main constituent parts and note the updates that are important for this particular study.

The data is obtained by solving the system of equations, describing the co-evolution of gas and dust. Both components are considered as fluids; however, dust is a pressureless fluid. The following key processes are taken into account: self-gravity of a disk (both gaseous and dusty); friction between dust and gas, including back-reaction of dust onto gas; and turbulent viscosity, which is introduced using the α-parametrization of Shakura–Sunyaev (Shakura and Sunyaev, 1973). The energy balance includes compressional heating or cooling, heating and cooling via radiation and viscous heating. The dust in the disk does not have a constant size, but is represented by an ensemble with a certain maximal size, locally determined by the processes of growth and fragmentation.

It was already mentioned above that we use the Shakura–Sunyaev parametrization of viscosity. The value of $\alpha_{\rm visc}$ is variable in space and time in our study. We adopt the layered disk model (Gammie, 1996) to choose the $\alpha_{\rm visc}$ value in a disk. The full description of the model can be found in Kadam et al. (2020). We assume the thickness of a disk which can be sufficiently ionized via cosmic rays is 100 g cm^{-2}. The threshold temperature required for thermal ionization of alkali metals is set to $T_{\rm crit}$ = 1300 K.

Finally, to simulate a flyby of the (sub-)solar mass object, we use the approach presented in Vorobyov et al. (2017), which allows for modeling of a coplanar encounter between a disk with a central source and an intruder perturbing a system.

We present the results of two computations: (i) a fiducial model representing a single-star system; and (ii) a perturbed model in which the intruder was launched toward the central source from a distance of 3000 au. The initial intruder velocity has two components: radial velocity $v_{\rm r} = -2.5$ km s^{-1} (note that the negative value accounts for the motion toward the central star) and azimuthal velocity $v_\phi = 0.2$ km s^{-1}. The encounter is retrograde, which means that the intruder motion is opposite to the star (and disk) rotation. The intruder mass is $M_{\rm int} = 0.5$ M$_\odot$. The computational domain covers the region of 3500×3500 au^2 divided into 400×256 cells in the radial and azimuthal direction, respectively.

2.2 Initial configuration

The disk and conditions there at the beginning of each run are the same. Initial distributions of gas, temperature, and viscosity parameter $\alpha_{\rm visc}$ are shown in Fig. 1. Clearly, the disk has a well-defined spiral structure, i.e., it is gravitationally unstable. The initial point of simulation is approximately 100 kyr after the disk formation via gravitational collapse. Thus, the disk is still in the active embedded phase of evolution when the development of gravitational instability is expectable. The temperature distribution does not show azimuthal variations that would be significant, although some inhomogeneity does exist. The most dense inner disk is MRI-dead, and the corresponding decrease in $\alpha_{\rm visc}$ is notable there.

Focusing on the innermost disk, which is shown in the right column of Fig. 1, one would see the complex structure. There is a certain accumulation of matter around the inner

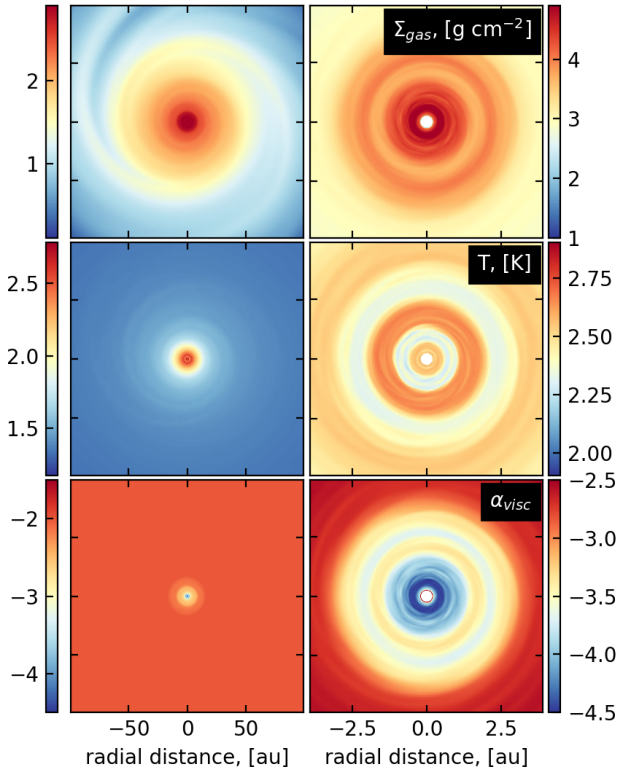

Fig. 1. Initial distribution of gas surface density (top row), temperature (middle row), and viscosity parameter $\alpha_{\rm visc}$ (bottom row). The left and right columns show the disk on different scales: the 100×100 au^2 box and the innermost part of the disk within the 4×4 au^2 area, respectively. All the values are shown in the log scale.

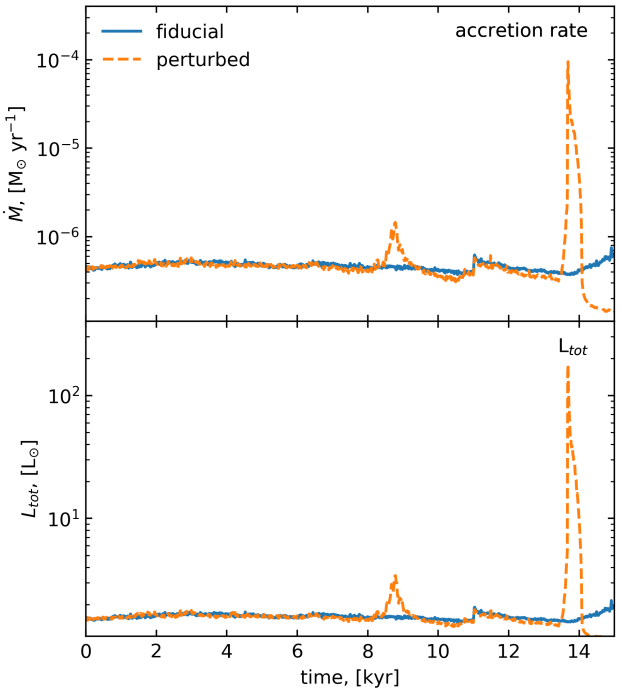

Fig. 2. Accretion rate and total luminosity as functions of time are shown in the top and bottom panels, respectively. Blue curves correspond to the fiducial model; orange, to the model with the intruder.

boundary and the ring structure at approximately 2 au. The temperature of the ring is lower than that of its surroundings. The peak of temperature is situated between the innermost accumulated matter and the gaseous ring, in the region where both viscosity and gas surface density are high, thus facilitating the viscous heating. $\alpha_{\rm visc}$ starts to decrease at $r \sim 2.5$ au, and closer to the star it reaches low ($\alpha_{\rm visc} \leq 10^{-2}$) values corresponding to a completely MRI-dead zone. Clearly, the gas accumulation occurs where $\alpha_{\rm visc}$ has a sharp decrease (in the outside–inside direction) because the capability of mass transport via viscous torque changes. If a higher viscosity zone surrounds a zone with a lower one, then an excess of matter that cannot be transported accumulates at the interface between zones. More details on the process can be found in Kadam et al. (2020).

The modeling starts from the presented distribution, and then the intruder changes it via gravitational interaction, while the fiducial model evolve freely without perturbation, serving as a reference case.

2.3 Origin of luminosity peaks

The work aims to study the possibility of luminosity burst development caused by a flyby of an external object. Once the intruder launched in the perturbed model simulation, it

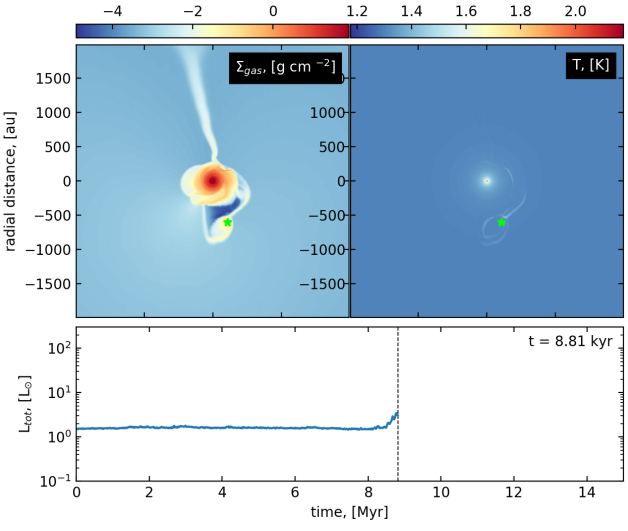

Fig. 3. Perturbed model during the luminosity rise following the moment of periastron passage. The top row of panels shows the spatial distribution of gas surface density (left column) and midplane temperature (right column). Values are shown in the 2000×2000 au^2 area at $t = 16.67$ kyr since the intruder launch. Colors are in the log scale. The total luminosity of the central star as a function of time is shown in the bottom panel. The vertical dashed line marks the current time instant.

took 7.95 kyr to reach the point of the closest approach, with a periastron of $d \simeq 500$ au. However, no significant changes in luminosity have taken place by that moment, as it is clearly seen in Fig. 2. The accretion rate and, consequently, the luminosity increase, peaking at $t = 8.81$ kyr. Despite the luminosity increased by two times, it is too low for a FUor. The next accretion and luminosity peak occurs almost 5 kyr later, and the peak luminosity is two orders of magnitude higher than the preceding quiescent luminosity.

First, we consider the luminosity increase that follows the closest approach. By the time the luminosity reaches its first peak, the intruder has already gone 50 au farther, and the increase in accretion rate is a consequence of the first perturbation finally penetrated through the disk. The gaseous disk structure is shown in Fig. 3. The track of the intruder is clearly observable, as the intruder gravitationally gathers matter from its surroundings during its movement and leaves the characteristic pre-collisional tail-like structure and the post-collisional tail-like structure. The intruder also has its own disk of lower density and size (this picture is in consistence with the results obtained in Vorobyov et al. (2020)). The tail-like structures are not stable, but curve and accrete onto the disk along with the matter from the envelope. The front of the post-collisional tail-like structure is warmer compared to the surrounding medium due to compressional heating because it is actually the shock front. The form of the disk is a bit flattened. Although the two-times luminosity increase, the disk temperature is not much affected.

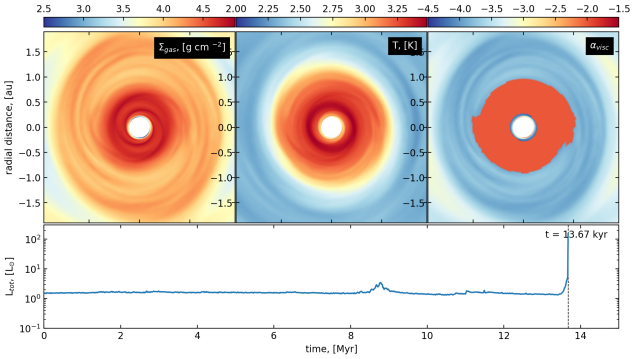

Fig. 4. Configuration of the inner disk part (2×2 au^2) in the perturbed model at the moment of the MRI burst ($t = 13.67$ kyr). Spatial distributions of the gas surface density, midplane temperature, and viscosity parameter $\alpha_{\rm visc}$ are shown in the top row of panels by colors in the log scale. The bottom panel is similar to that of Fig. 3.

The situation changes when considering the second accretion enhancement event, which arises almost 5 kyr after the previous one. Despite the intruder is $\simeq 2500$ au away, the inner disk at the moment of the second luminosity burst differs from the initial configuration qualitatively and quantitatively, as it is evident from Fig. 4. The gaseous rings have disappeared, the inner gaseous disk structure is noticeably asymmetric (in contrast to the initial almost-axisymmetric configuration), while a certain ring-like structure is still retained in the temperature distribution. The temperature values are up to an order of magnitude higher than the initial ones.

The most important part that sheds light on the root of accretion rate enhancement is the distribution of $\alpha_{\rm visc}$. A sharp increase in the turbulent viscosity parameter up to $\alpha_{\rm visc} \simeq 10^{-2}$ takes place where the dead zone was established initially. This sharp increase is undoubtedly the consequence of the MRI development. Nevertheless, it remains unknown what was the first: the luminosity burst, which further increased the temperature up to the threshold value $T_{\rm crit} = 1300$ K, or MRI development – the only source of the accretion enhancement.

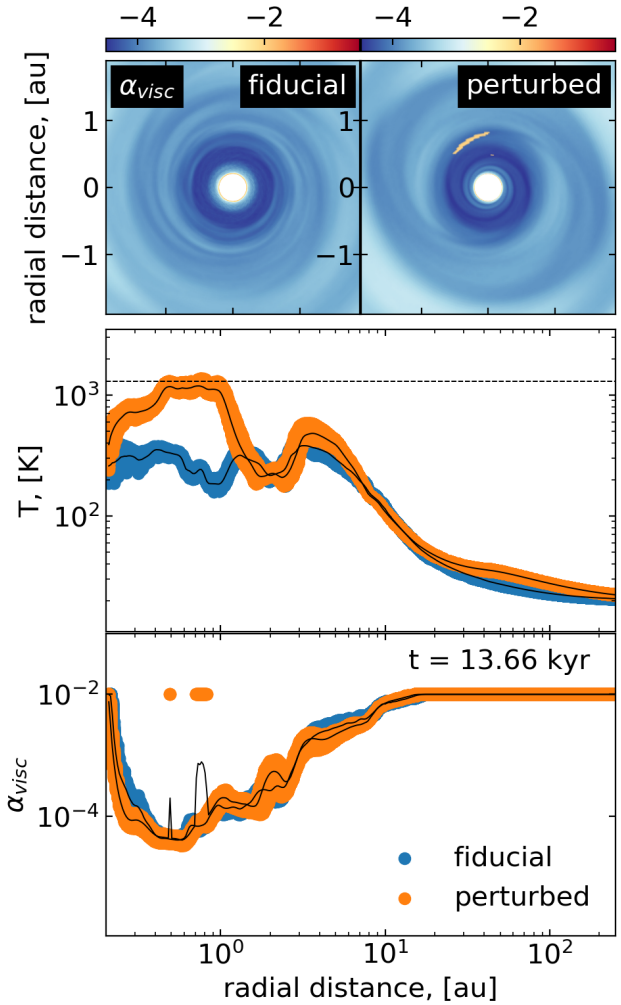

Fig. 5. Innermost disk immediately before the accretion luminosity burst ($t = 13.66$ kyr). The spatial distribution of $\alpha_{\rm visc}$ is shown in the top row of panels. Colors are in the log scale. The middle panel presents the midplane temperature as a function of radius. Thick dots correspond to all the azimuthal temperature values at a given radius. Black solid lines show the azimuthally averaged values. Azimuthal variations in $\alpha_{\rm visc}$ as a function of radius are shown in the bottom panel.

Considering the pre-burst condition of the system, it becomes obvious that the development of MRI occurs prior to the luminosity increase. The distribution of $\alpha_{\rm visc}$ is presented in Fig. 5 together with the azimuthal variations of $\alpha_{\rm visc}$ as a

function of radius. The small region at $r = 1$ au is fully MRI-active, i.e., $\alpha_{\rm visc} \geq 10^{-2}$. Clearly, the MRI triggers where the temperature exceeds $T_{\rm crit} = 1300$ K, which assumed to be high enough for the thermal ionization of matter. Thus, the intruder-induced perturbation leads to a burst of accretion due to the development of the MRI in the system.

3 Conclusions

We numerically simulated a close encounter between a star with a surrounding disk and an external intruder object of sub-solar mass. The collision was coplanar, and the setup with an expectedly large (hundreds of au) periastron was used. To evaluate an effect of the intruder onto accretion characteristics of the target disk, the reference model without a perturbing object was also computed. Our findings can be summarized as follows.

- It was shown that the luminosity burst with characteristics resembling those of a FUor object can occur in binaries with stars situated far beyond tens of au and doesn't require low periastron.
- The first perturbation, developed due to the encounter of two stars with a large ($\simeq$ 500 au) periastron, takes at least hundreds (700+) of years to reach the target star.
- Such a perturbation can disbalance the disk, which finally results in the development of the MRI, providing a significant increase in the rate of mass accretion and thus accretion luminosity, appearing as a FUor. The time elapsed from the closest approach to the MRI ignition is more than 4000 years. This means that the encounter can trigger a burst even thousands of years after the event itself.

Acknowledgements. This work was supported by the Theoretical Physics and Mathematics Advancement Foundation "BASIS" grant 21-1-5-95-1.

References

Armitage P.J., Livio M., Pringle J.E., 2001. Mon. Not. Roy. Astron. Soc., vol. 324, no. 3, pp. 705–711.

Audard M., Ábrahám P., Dunham M.M., et al., 2014. In H. Beuther, R.S. Klessen, C.P. Dullemond, T. Henning (Eds.), Protostars and Planets VI. p. 387. doi:10.2458/azu_uapress_9780816531240-ch017 (arXiv:1401.3368).

Banzatti A., Pinilla P., Ricci L., et al., 2015. Astrophys. J. Lett., vol. 815, no. 1, p. L15.

Connelley M.S., Reipurth B., 2018. Astrophys. J., vol. 861, no. 2, p. 145.

Gammie C.F., 1996. Astrophys. J., vol. 457, p. 355.

Kadam K., Vorobyov E., Regály Z., Kóspál Á., Ábrahám P., 2020. Astrophys. J., vol. 895, no. 1, p. 41.

Kenyon S.J., 1999. In C.J. Lada, N.D. Kylafis (Eds.), The Origin of Stars and Planetary Systems. NATO Advanced Study Institute (ASI) Series C, vol. 540, p. 613 (arXiv:astro-ph/9904035).

Liu H.B., Vorobyov E.I., Dong R., et al., 2017. Astron. Astrophys., vol. 602, p. A19.

Mercer A., Stamatellos D., 2017. Mon. Not. Roy. Astron. Soc., vol. 465, pp. 2–18.

Molyarova T., Akimkin V., Semenov D., et al., 2018. Astrophys. J., vol. 866, no. 1, p. 46.

Nayakshin S., Lodato G., 2012. Mon. Not. Roy. Astron. Soc., vol. 426, no. 1, pp. 70–90.

Pérez S., Hales A., Liu H.B., et al., 2020. Astrophys. J., vol. 889, no. 1, p. 59.

Pfalzner S., 2008. Astron. Astrophys., vol. 492, no. 3, pp. 735–741.

Rab C., Elbakyan V., Vorobyov E., et al., 2017. Astron. Astrophys., vol. 604, p. A15.

Schoonenberg D., Ormel C.W., 2017. Astron. Astrophys., vol. 602, p. A21.

Shakura N.I., Sunyaev R.A., 1973. Astron. Astrophys., vol. 24, pp. 337–355.

Visser R., Bergin E.A., Jørgensen J.K., 2015. Astron. Astrophys., vol. 577, p. A102.

Vorobyov E.I., 2009. Astrophys. J., vol. 704, no. 1, pp. 715–723.

Vorobyov E.I., Akimkin V., Stoyanovskaya O., Pavlyuchenkov Y., Liu H.B., 2018. Astron. Astrophys., vol. 614, p. A98.

Vorobyov E.I., Basu S., 2015. Astrophys. J., vol. 805, p. 115.

Vorobyov E.I., Elbakyan V.G., Liu H.B., Takami M., 2021. Astron. Astrophys., vol. 647, p. A44.

Vorobyov E.I., Skliarevskii A.M., Elbakyan V.G., et al., 2020. Astron. Astrophys., vol. 635, p. A196.

Vorobyov E.I., Skliarevskii A.M., Molyarova T., et al., 2022. Astron. Astrophys., vol. 658, p. A191.

Vorobyov E.I., Steinrueck M.E., Elbakyan V., Guedel M., 2017. Astron. Astrophys., vol. 608, p. A107.

Wiebe D.S., Molyarova T.S., Akimkin V.V., Vorobyov E.I., Semenov D.A., 2019. Mon. Not. Roy. Astron. Soc., vol. 485, no. 2, pp. 1843–1863.